Totally asymmetric simple exclusion process with local resetting in a resource-constrained environment

Nikhil Bhatia and Arvind Kumar Gupta*
Department of Mathematics, Indian Institute of Technology Ropar Punjab, India

(Received 27 October 2023; accepted 22 January 2024; published 13 February 2024)

Inspired by the process of mRNA translation, in which the stochastic degradation of mRNA-ribosome machinery is modeled by the resetting dynamics, we study an open totally asymmetric simple exclusion process with local resetting at the entry site in a resource-constrained environment. The effect of constrained resources on the stationary properties of the system has been comprehended in the form of the filling factor. The mean-field approximations are utilized to obtain stationary state features, such as density profiles and phase diagrams. The phase diagram possesses pure phases as well as coexisting phases, including a low-density–high-density phase separation, which did not manifest under periodic boundary conditions despite the system being closed there as well. The role of the resetting rate has been investigated on the stationary properties of the system, depending on how the filling factor scales with the system size. In contrast to the resetting model for infinite resources, two distinct phase transitions are observed for the smaller values of the filling factor leading to a change in the topology of the phase diagram. The impact of the resetting rate along with the finite-size effect has also been examined on the shock dynamics. All the mean-field results are found in remarkable agreement with the Monte Carlo simulations.

DOI: 10.1103/PhysRevE.109.024109

I. INTRODUCTION

Transport, being a universal phenomenon, falls in the domain of nonequilibrium statistical physics and is ubiquitous, starting from the microscopic world of cellular processes to macroscopic vehicular flow, etc. Some intriguing examples of such systems range from man-made to natural systems, including traffic flow in vehicles, biological transport mechanisms, pedestrian movement, etc. [1–4]. While the long-term behavior of their counterparts can be comprehended through a unified theory attributed to Boltzmann and Gibbs [5], nonequilibrium systems, employed to represent a broader spectrum of natural phenomena, remain less understood in terms of their behavior. The nonequilibrium systems have constant contact with the net driving force acting upon them and tend to remain in nonequilibrium [6]. These systems undergo evolution based on rules that defy detailed balance, and their distinctive characteristic is the presence of a nonzero current in a steady state. A significant challenge with such systems is that, despite showcasing complex behaviors like phase transition and phase separation, all these characteristics are defined by a time-independent state referred to as nonequilibrium steady states (NESS) [7,8].

A mathematically tractable model that provides a framework in which issues of NESS are well-posed and captured is the totally asymmetric simple exclusion process (TASEP) [4,9–12]. It captures the essence of many particle nonequilibrium systems interacting with each other on a one-dimensional lattice with the help of random walkers that can hop unidirectionally and follow the hard-core exclusion principle. From an analytical point of view, the exact solvability of TASEP serves as an archetype for the studies of systems where underlying physical principles involve NESS [13–19]. The dynamics of the model in NESS are crucially sensitive to the boundary conditions and develop a complex phase diagram controlled by the system's interactions with its environment. For a system with periodic boundary conditions, the stationary state is trivial, with all configurations having equal probability (i.e., a flat distribution) [9]. In contrast, the open boundary conditions produce distinct phases including an entry-dominated (or low-density), an exit-dominated (or high-density), a maximal-current phase as well as exhibits a delocalized shock on the transition line between the low-density and high-density phases. Moreover, it captures richer phenomena such as boundary-induced phase transitions [20–22], etc. In open systems, the entry and exit rates are controlled by considering the particle reservoirs having constant densities at the left and right boundaries [7].

TASEP being a minimal model to study stochastic transport has been extended to incorporate realistic features among various transport systems [23–26]. One such generalization is the TASEP with Langmuir kinetics (TASEP-LK) where particles can attach to or detach from the one-dimensional lattice [27]. It integrates the equilibrium process namely Langmuir kinetics (LK) dynamics represents the attachment and detachment of particles on a lattice with the nonequilibrium process TASEP. This model comprehends various complex features at a stationary state such as a rich phase diagram, with high and low-density phases, two and three-phase coexistence regions, a boundary-independent Meissner phase, and a localized domain wall leading to a low-high coexistence phase [28–30].

*akgupta@iitrpr.ac.in

To model the observables in various real-life dynamical systems that are interrupted and resumed from a certain point in the phase space, the diffusion process in the conventional TASEP is accompanied by a nonequilibrium process called stochastic resetting. For example, resetting the Brownian particle to its initial position with some fixed rate [31]. This simple act of resetting leads to many nontrivial findings, such as nontrivial stationary state, nonmonotonic mean first passage time, etc. In recent times, the concept of stochastic resetting dynamics has been applied to address several microbiological issues such as the interplay of degradation of random mRNA and ribosome loading of mRNA in the translation process [32]. It has many further applications, ranging from the search and optimization algorithms [33], predator-prey system model [34], chemical reactions [35], and biopolymerization [36], etc. Stochastic resetting occurs in two ways either global or local. Much of the literature has already been vigorously explored under the global aspect - where resetting is either applied to a single degree of freedom or it is simultaneously applied to multiple degrees of freedom [37–40]. Local resetting where particles can reset their position independently of one another is more challenging than the global resetting considered, where the whole system is simultaneously reset to some reference state. The local resetting was first introduced and investigated in a symmetric simple exclusion process with periodic boundary conditions [41,42]. The analysis was then extended to the TASEP with periodic boundary conditions, showing that the intermediate resetting regime arises for the resetting rate of the order inverse lattice length [41,42]. A similar situation is observed in the TASEP-LK model, where the attachment-detachment rates of particles are rescaled in the order of the inverse lattice length to observe the competition between boundary and bulk dynamics. This highlights a crucial connection between the resetting process and the LK dynamics, demonstrating how the resetting process is a unique instance of the LK process in which only the detachment process is present (from the bulk of the system) [41,42].

Many TASEP models and their extensions are based on the assumption that the system is connected to an infinite reservoir [43], despite the fact that many physical systems in nature, such as ribosomes in a cell for protein synthesis, vehicles in the context of traffic, pedestrian traffic or filament length kinetics, all these compete for resources in a pool of limited availability [44–46]. To take into account the impact of restricted availability of resources, studies have lately been expanded by linking a finite reservoir (or pool) to the open TASEP [47–52]. In contrast to the open TASEP connected to an infinite reservoir, the particles remain conserved in the system with a finite pool and the system exhibits a novel feature such as the transition line separating the low-density and high-density phases is expanded to a region where a localized domain wall is formed [53–55].

While much of the literature has focused on TASEP models with stochastic resetting, either in open boundary conditions or with periodic boundary conditions, most real-life systems, as discussed above, only compete in a finite pool of resources. Our interest here is to review work along this line of investigation by considering a TASEP with local resetting at the injection node under the availability of limited resources. The stationary state features will be studied theoretically using mean-field approximations and validated using Monte Carlo simulations. Our focus is to explore the consequences of the interplay between local resetting and the filling factor in the presence of finite resources and understand the stationary state behavior of the TASEP-LR in the thermodynamic limit.

In a manner similar to the original TASEP model, which serves as a model for simulating the movement of mRNA and ribosomes during protein synthesis [56], or the TASEP-LK model, which includes both attachment and detachment processes, thought to be a fundamental illustration of molecular motor dynamics on microtubules for intracellular transport processes [30]. As a result, our LR-inclusive model might be used as a mechanism for ribosome rescue and recycling or to address premature translation termination brought on by ribosome detachment prior to reaching the stop codon (drop-off phenomenon) [57,58]. The resetting node represents the mRNA site where ribosomes bind to start the translation.

II. MODEL DESCRIPTION

We consider a one-dimensional discrete lattice with L sites in which particles diffuse on the lattice as well as locally reset following the Markovian stochastic rules, (see Fig. 1). The lattice sites are labeled as $i = 1, 2, \ldots, L$, where $i = 1(L)$ represents the entry(exit), and the remaining sites $(i = 2, \ldots, L-1)$ are referred to as the bulk of the lattice. The open boundaries of the lattice are connected to a finite reservoir of particles from which the particles enter the lattice through the first site and rejoin the reservoir back through its last site. The particles on the lattice hop uni-directionally from left to right and the resetting phenomena of particles occur at the entry site only. Each lattice site adheres to the hardcore exclusion principle and follows the restriction that only one particle can occupy a lattice site. The proposed model can also be viewed as a periodic TASEP model having a special site that violates the exclusion principle.

The following describes the particle dynamics and the corresponding rates that take place at the entry, bulk, and exit lattice sites: If the entry site is occupied, then the particle hops to the site on the right with a unit rate, provided it is vacant. For an unoccupied entry site, a particle from the reservoir enters the first site with a rate α_{eff}. For an occupied bulk and exit site, the particle initially tries to reset itself with a rate r from this lattice site to the entry site, provided the entry site is vacant. Otherwise, the bulk particle will attempt to hop to its adjacent empty site on the right with a unit rate or if the particle is at the last site, then it returns to the reservoir with a rate β.

The proposed model is motivated by the dynamical aspects of the so-called drop-off phenomenon, which is the premature cessation of the translation process as a result of stalled ribosomes along with their rescue and recycling [56–58]. But from the theoretical point of view, our study is general and it may serve as a basis for more detailed investigations along the lines [57,59]. The model described in Fig. 1 can non-trivially be linked to the TASEP-LK model for some entry rate $\tilde{\alpha_{\text{eff}}}$, exit rate β, attachment rate $w_A = 0$ and detachment rate $w_D = r(1-\rho_1)$. Furthermore, in the proposed model, the reservoir can additionally be considered a unique lattice

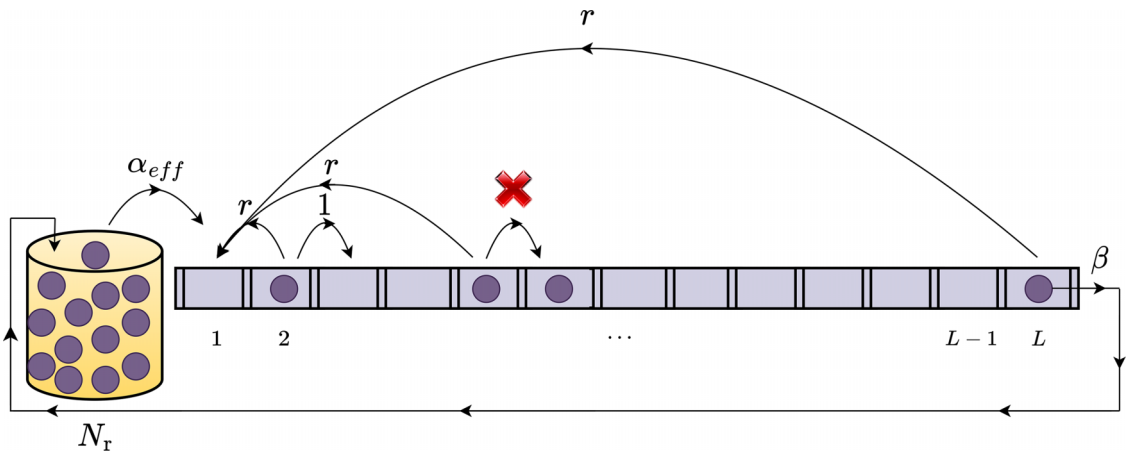

FIG. 1. Schematic diagram of the TASEP with local resetting at the entry site. The rate of each process is represented by a matching symbol, and it is believed that lattice sites are arranged from left to right. If the arrival site is unoccupied, then the hopping process has a unit rate; otherwise, it is prohibited (zero rate).

site connected to both ends of the lattice. Furthermore, the relation $\alpha_{\text{eff}} = \alpha g(N_r)$ is used to establish the effective entry rate, or α_{eff}, which is based on the number of particles in the reservoir (N_r). The system dynamics and the inflow rate of particles that is proportional to the number of particles in the reservoir are determined by the choice of g [47]. As a result, g can be thought of as a monotonically growing function, defined as $g(N_r) = \frac{N_r}{N_{\text{tot}}}$ where N_{tot} denotes the total number of particles in the system (lattice and reservoir combined). To investigate the impact of the total population of the particles relative to the size L of the lattice on the system dynamics, we utilize the notion of filling factor, which is defined as $\mu = \frac{N_{\text{tot}}}{L}$ [48]. It describes the average number of particles available for each lattice site and it lies in the range $[0, \infty)$. The limiting situation, $\mu \to \infty$, corresponds to the case of an infinite reservoir where the entry rate becomes a constant, i.e., $\alpha_{\text{eff}} = \alpha$.

III. THEORETICAL ANALYSIS UNDER MEAN-FIELD APPROXIMATION

Let τ_i be the binary random variable that specifies the occupational number for the ith lattice site since the lattice meets the exclusion requirement. The random variable τ_i takes the value 0 or 1 depending on whether the site is occupied or unoccupied. The following master equation describes the evolution of the average site occupancy number in the bulk of the lattice ($2 \leqslant i \leqslant L-1$):

$$\frac{d\langle\tau_i\rangle}{dt} = \langle\tau_{i-1}(1-\tau_i)\rangle - \langle\tau_i(1-\tau_{i+1})\rangle - r\langle(1-\tau_1)\tau_i\rangle. \quad (1)$$

The first two terms in the above equation represent the gain and loss current due to particle hopping whereas the third term also represents a loss term due to the resetting process of the particle in the bulk. The average site occupancy number changes at the lattice boundaries in accordance with the following equations:

$$\frac{d\langle\tau_1\rangle}{dt} = \alpha_{\text{eff}}\langle(1-\tau_1)\rangle - \langle\tau_1(1-\tau_2)\rangle + r\left\langle(1-\tau_1)\sum_{i=2}^{L}\tau_i\right\rangle, \quad (2)$$

$$\frac{d\langle\tau_L\rangle}{dt} = \langle\tau_{L-1}(1-\tau_L)\rangle - \beta\langle\tau_L\rangle - r\langle(1-\tau_1)\tau_L\rangle. \quad (3)$$

Due to the existence of one- and two-point correlators, the aforementioned system of equations cannot be directly solved. Therefore, we utilize the mean-field approximation, which ignores any potential correlations inherent in the aforementioned set of equations, i.e., $\langle\tau_i\tau_j\rangle = \langle\tau_i\rangle\langle\tau_j\rangle$.

Now, to understand the behavior in the bulk of the system in its continuum limit (or thermodynamic limit), we coarse grain the lattice by introducing a quasicontinuous position variable $x = \frac{i}{L} \in [0, 1]$, the lattice constant as $\epsilon = \frac{1}{L}$ and a rescaled time $t' = \frac{t}{L}$.

Replacing the binary discrete variable τ_i with a continuous local average density at i^{th} site as $\rho_i = \langle\tau_i\rangle \in [0, 1]$ and retaining the terms up to the first order of ϵ in the Taylor series expansion of $\rho(x \pm \epsilon)$ and substituting it in the density evolution Eq. (1) for the bulk. Further, we drop the subscript i due to the spatial homogeneity on the lattice to reform Eq. (1) into

$$\frac{\partial\rho}{\partial t'} + \frac{\partial J}{\partial x} = -\lambda\rho, \quad (4)$$

where $\lambda = R(1-\rho_1)$, $R = rL$ is the modified resetting rate and $J = \left(-\frac{\epsilon}{2}\frac{\partial\rho}{\partial x} + \rho(1-\rho)\right)$ denotes the average particle current in the bulk of the lattice for a finite ϵ, whereas in the thermodynamic limit ($\epsilon \to 0^+$), it becomes $J = \rho(1-\rho)$. The following can explain the necessity of introducing a modified resetting rate: the struggle between bulk and boundary dynamics in large systems will only be evident if particles get enough time to spend on the lattice before resetting themselves to the first site, therefore, a macroscopic resetting rate R is introduced, which remains constant for $L \to \infty$. The macroscopic resetting rate R is a crucial variable whose

behavior in the thermodynamic limit $L \to \infty$ establishes the importance of the resetting process in comparison to conventional TASEP.

On similar grounds, the master equation for boundary conditions is reformed into

$$\frac{d\rho_1}{dt} = \alpha_{\text{eff}}(1-\rho_1) + r(1-\rho_1)\sum_{i=2}^{L}\rho_i - \rho_1(1-\rho_2), \quad (5)$$

$$\frac{d\rho_L}{dt} = \rho_{L-1}(1-\rho_L) - \beta\rho_L - r(1-\rho_1)\rho_L. \quad (6)$$

In the following, we shall drop the time index to focus on the stationary state of the differential Eq. (4) and obtain

$$\frac{\partial J}{\partial x} = -\lambda\rho. \quad (7)$$

Integration of the above equation w.r.t. x yields

$$\rho(x)\exp(-2\rho(x)) = \rho(x_0)\exp(-2\rho(x_0) - \lambda(x-x_0)), \quad (8)$$

where x_0 is some reference point that can assume the value 0 or 1 corresponding to the left and right boundary sites, respectively. Equation (8) has an explicit solution for particle density in terms of the Lambert-W function [60] given by

$$\rho(x) = -\tfrac{1}{2}W(-2\rho(x_0)\exp(-2\rho(x_0) - \lambda(x-x_0)). \quad (9)$$

The function $W(x)$ is a multivalued function that has two real branches $W_0(x)$ and $W_{-1}(x)$. The branch $W_0(x)$ is defined for $x \geqslant -1/e$ whereas $W_{-1}(x)$ is defined for $-1/e \leqslant x \leqslant 0$ and both the branches meet at $x = -1/e$. The branch $W_0(x)$ ($W_{-1}(x)$) is bound within the interval $[-1, \infty]$ ($[-\infty, -1]$) and corresponds to the $\rho(x) \leqslant 1/2$ ($\rho(x) \geqslant 1/2$).

At stationary state, the density solution in an entry-dominated low-density phase is obtained by matching the boundary condition on the left end, i.e., $\rho(x=0) = \rho_1$ and is written as

$$\rho_{\text{LD}}(x) = -\tfrac{1}{2}W_0(-2\rho_1\exp(-2\rho_1 - \lambda x)), \quad (10)$$

whereas the boundary condition on the right end, i.e., $\rho(x = 1) = 1 - \beta$ is utilized to obtain the density solution in an exit-dominated high-density phase and is given by

$$\rho_{\text{HD}}(x) = -\tfrac{1}{2}W_{-1}(-2(1-\beta)\exp(-2(1-\beta) + \lambda(1-x))). \quad (11)$$

Note that the density solution in the LD (HD) phase given by Eq. (10) [Eq. (11)] clearly satisfies the left (right) boundary condition as well as matches in the bulk. However, due to the presence of boundary layers, these expressions do not satisfy the right (left) boundary, respectively. The stationary state density solution in the maximal current phase is specified by the condition: $\rho(x=0) = \frac{1}{2}$ and is obtained as

$$\rho_{\text{MC}}(x) = -\tfrac{1}{2}W_0(-\exp(-1-\lambda x)). \quad (12)$$

Till now, we have discussed the density profiles in one of the three following phases, namely, low-density (LD), high-density (HD), and maximal-current (MC) phases. Further, there may be the possibility of having the bulk density as the combination of the above-mentioned phases which can be obtained utilizing the current continuity principle and depending on how the combination of the above-obtained solutions is matched [30]. Taking into account the nature of phases, there are a total of twelve possible combinations of coexisting phases. However, the current-continuity principle restricts to only two possible coexisting phases: an LD-HD phase and an MC-HD phase both representing a localized shock in the lattice. Now, we analyze the aforementioned phases theoretically to obtain the density profiles and the existence conditions.

The density profile exhibiting the coexistence of the LD and HD phase is given by:

$$\rho_{\text{LD-HD}}(x) = \begin{cases} \rho_{\text{LD}}(x); & 0 \leqslant x \leqslant x_w, \\ \rho_{\text{HD}}(x); & x_w \leqslant x \leqslant 1, \end{cases} \quad (13)$$

whereas the density profile representing the coexistence of the MC and HD phase is given by

$$\rho_{\text{MC-HD}}(x) = \begin{cases} \rho_{\text{MC}}(x); & 0 \leqslant x \leqslant x_w, \\ \rho_{\text{HD}}(x); & x_w \leqslant x \leqslant 1. \end{cases} \quad (14)$$

Here, the x_w corresponds to the position of the shock in the coexistence phases LD-HD phase and MC-HD phase. It can be obtained utilizing the fact that in both cases the density jumps from $\rho(x_w) < 1/2$ to $1 - \rho(x_w) > 1/2$ maintaining the current continuity. Hence, the domain-wall position x_w along with the density $\rho(x_w)$ can be obtained from conditions $\lim_{x\to x_w^-}\rho(x) = \rho(x_w)$ and $\lim_{x\to x_w^+}\rho(x) = 1-\rho(x_w)$, which together can be reformed into the relation given as

$$W_0(-2\rho_1\exp(-2\rho_1 - \lambda x_w)) - W_{-1}(-2(1-\beta) \times \exp(-2(1-\beta) + \lambda(1-x_w))) = 2, \quad (15)$$

where the numerical value of ρ_1 clearly depends on the choice of the coexisting phase. The expression for the height of the shock is given as

$$\Delta = \rho_{\text{HD}}(x_w) - \rho_{\text{LD}}(x_w). \quad (16)$$

The following set of equations is utilized to determine ρ_1 in each stationary phase:

$$\rho(0)\exp(-2\rho(0)) = \rho(1)\exp(-2\rho(1) - 1) \quad (17)$$

and

$$\alpha_{\text{eff}}(1-\rho_1) = \rho(1)(1-\rho(1)). \quad (18)$$

Equation (17) is a direct implication from Eq. (8), whereas Eq. (18) follows from the current-continuity principle. Table I lists the phase boundaries computed using the extremal current principle as well as the boundary densities [10,61]. The upcoming section will explore the steady-state features like density profiles and phase diagrams of the lattice.

IV. EXISTENCE OF STATIONARY PHASES AND PHASE BOUNDARIES UNDER THE COMPETITION OF FINITE RESOURCES

The assumption of finite resources in the reservoir only affects the entry rate of particles, whereas the exit rate of particles is independent of N_r. It is assumed that the free particles in the reservoir are homogeneously distributed and not correlated within the reservoir. To determine the modified entry rate (α_{eff}), the conservation of the number of particles in the system is utilized, which in its continuum form states that $N_{\text{tot}} = N_r + L\int_0^1 \rho(x)\,dx$. Since the dynamics pertaining to

TABLE I. Expressions for the existence conditions of the density phases in the lattice with finite resources through mean-field theory.

Density Phase		Phase Region
LD	$\alpha_{\text{eff}} < -W_0\big(-\exp\big(-\big(1+\frac{R}{2}\big)\big)\big)\big(1+\frac{1}{2}W_0\big(-\exp\big(-\big(1+\frac{R}{2}\big)\big)\big)\big)$,	$\alpha_{\text{eff}} < \frac{\beta(1-\beta)}{1-\frac{1}{(R-2)}W_0((R-2)\beta\exp(R-2\beta))}$.
HD	$\alpha_{\text{eff}} > \frac{\beta(1-\beta)}{-\frac{1}{(R+2)}W_{-1}((-R-2)(1-\beta)\exp(2\beta-2))}$,	$\alpha_{\text{eff}} > \frac{\beta(1-\beta)}{-\frac{1}{R}(1-2\beta-\ln(2-2\beta))}$.
MC	$\alpha_{\text{eff}} > -W_0\big(-\exp\big(-\big(1+\frac{R}{2}\big)\big)\big)\big(1+\frac{1}{2}W_0\big(-\exp\big(-\big(1+\frac{R}{2}\big)\big)\big)\big)$,	$\alpha_{\text{eff}} < \frac{\beta(1-\beta)}{\frac{1}{R}(2\beta-1-\ln(2\beta))}$.
LD-HD	$\alpha_{\text{eff}} > \frac{\beta(1-\beta)}{1-\frac{1}{(R-2)}W_0((R-2)\beta\exp(R-2\beta))}$,	$\alpha_{\text{eff}} < \frac{\beta(1-\beta)}{-\frac{1}{(R+2)}W_{-1}((-R-2)(1-\beta)\exp(2\beta-2))}$.
MC-HD	$\alpha_{\text{eff}} < \frac{\beta(1-\beta)}{-\frac{1}{R}(1-2\beta-\ln(2-2\beta))}$,	$\alpha_{\text{eff}} > \frac{\beta(1-\beta)}{\frac{1}{R}(2\beta-1-\ln(2\beta))}$.

the reservoir significantly affect the system, we define $\rho_{\text{r}} = \frac{N_{\text{r}}}{L}$ to be the density of the reservoir and utilize particle number conservation to retrieve the following relationship:

$$\mu = \rho_{\text{r}} + \int_0^1 \rho. \tag{19}$$

Considering the fact that the lattice can accommodate a maximum of L particles, the standard open-TASEP with local resetting (corresponding to infinite particles) is approached when $N_{\text{tot}} \gg L$. The interplay of the finite reservoir and resetting comes into play when the total number of particles in the system is of the order of $N_{\text{tot}} \sim L$ or smaller [52]. So far, we have deduced that there are five possible stationary phases that can exist in the phase diagram. Now, we utilize Eq. (19) with the results obtained in the previous section to derive the condition for the existence of the above-discussed stationary state phases in the presence of finite resources. Clearly, the explicit form of existence conditions is difficult to obtain for all the phases but the following implicit relation is ensured for the existence of a stationary phase:

$$\rho_{\text{r}} = \mu - \int_0^1 \rho(x)dx, \tag{20}$$

where $\rho(x)$ denotes the density profile to the corresponding stationary phase. In the next section, we will utilize the numerical methods to solve Eq. (4) along with Eqs. (5) and (6).

V. SIMULATIONS

In the previous section, we obtained the density profile and condition for the existence of phases in the implicit form using the Lambert-W function. In this section, first, we would like to provide a numerical scheme that can be used to solve the system of coarse-grained differential Eqs. (4), (5), and (6). Moreover, this scheme can also be utilized for the extended or generalized version of the proposed model. The differential equations (or continuum master equations) for which the numerical scheme is adopted are derived using the mean-field approximations; hence, we also utilize the Monte Carlo simulations to validate these approximations and compute the steady-state density profiles and the average current.

A. Direct simulation

We have obtained a generalized analytical formulation of the density profile at the stationary state [Eq. (9)]. Now, we provide an alternative method to obtain the numerical solution to the second-order continuum mean-field equation [Eq. (4)]. An important aspect of providing the numerical scheme is that the computation of the stationary state reservoir density ρ_R utilizing the system of Eqs. (20) and (2) make the problem complex as Eq. (2) itself is dependent on the local densities of all other sites. The time derivative is retained in the system and the density solutions at a steady state are procured in the limit $t \to \infty$. In this numerical solution, the geometric domain is discretized into grid points of the form $(i\triangle x, n\triangle t')$, where $\triangle x = 1/L$ and $\triangle t'$ are the grid spacing corresponding to the spatial and temporal variables, respectively. Assuming ρ_i^n as the numerical approximation of the particle density at each grid point, we utilize the forward-in-time and central-in-space (FTCS) scheme to obtain the finite-difference equation corresponding to differential Eq. (4) as

$$\rho_i^{n+1} = \rho_i^n + \triangle t'\bigg(\frac{\epsilon}{2}\bigg(\frac{\rho_{i+1}^n - 2\rho_i^n + \rho_{i-1}^n}{\triangle x^2}\bigg) + \bigg(\frac{\rho_{i+1}^n - \rho_{i-1}^n}{2\triangle x}\bigg)(2\rho_i^n - 1) - R(1-\rho_1)\rho_i^n\bigg). \tag{21}$$

Analogously, Eqs. (2) and (3) are utilized to obtain the finite-difference equations at the left and right boundary, respectively, as

$$\rho_1^{n+1} = \rho_1^n + L\triangle t'\bigg((1-\rho_1^n)\bigg(\alpha + r\sum_{i=2}^{L}\rho_i^n\bigg) - \rho_1^n(1-\rho_2^n)\bigg). \tag{22}$$

and

$$\rho_L^{n+1} = \rho_L^n + L\triangle t'\big(\rho_{L-1}^n(1-\rho_L^n) - \rho_L^n(\beta + r(1-\rho_1^n))\big). \tag{23}$$

The above system of explicit finite difference scheme will be stable against small amplitude perturbations for $\triangle t'/\triangle x^2 \leqslant 1$.

B. Monte Carlo simulations

As the implicit density profile computed in Secs. III and IV, and the density obtained via direct simulation utilizes mean-field approximation. To validate them, we perform Monte Carlo simulations using a Gillespie algorithm with a random sequential update rule [62]. Each step of the algorithm consists of choosing an event in accordance with the dynamical rules as defined in Sec. II. An event (a particle attempts to hop or resets to the first site) is selected with a probability proportional to the rates. Accordingly, the time increments

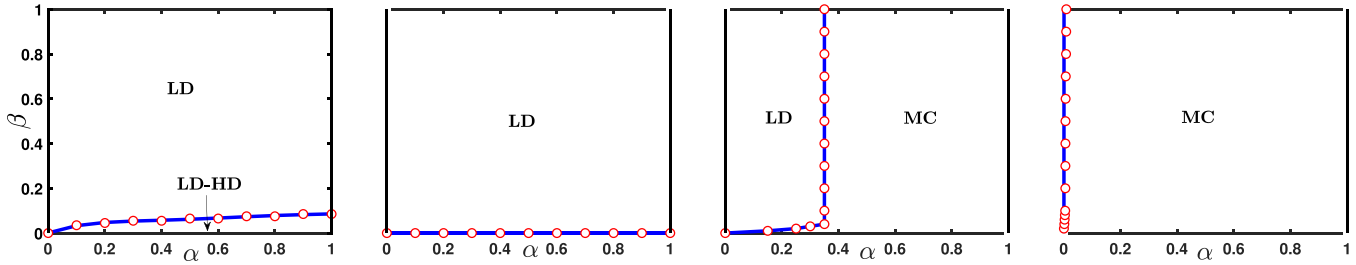

(a) $R = 0.03$ (b) $R = 5$ (c) $R = 6$ (d) $R = 10$

FIG. 2. Stationary state phase diagrams for $\mu = 0.1$ and different values of R. The markers are results from Monte Carlo simulations (MCS) and the solid lines are results from a continuum mean-field (CMF) approximation. The transition from LD to the LD-HD phase is discontinuous, resulting in a first-order transition. The transition from LD to the MC phase displays a continuous transition and hence is a second-order phase transition.

are chosen from exponentially distributed random numbers. The lattice length is taken to be $L = 500$ and the simulations are run for 10^8 time steps. To facilitate the onset of a steady state, we ignore the first 5% of time steps and the average particle density is calculated for an interval of $10L$. The results wherever obtained from Monte Carlo simulations are denoted by markers.

VI. RESULTS AND DISCUSSION

In the following section, we investigate the influence of the filling factor and the resetting rate on the phase diagrams which will further be utilized to scrutinize their impact on the stationary properties of the system.

A. Phase diagram: Role of filling factor and resetting rate

We derive the phase diagrams in the α-$\beta \in [0, 1] \times [0, 1]$ parameter space using the results discussed in the previous sections to study the role of the total number of particles and the macroscopic resetting rate on the stationary properties of the system. The resetting dynamics in the bulk and the boundary-induced nonequilibrium dynamics mutually interact and, eventually, produce collective effects if the particles stay long enough on the lattice before resetting to the first site. Hence, it is expected that R plays a crucial role in the topology of the phase diagram. However, the filling factor μ represents the average number of particles available for each lattice site, and due to the global constraint on the number of particles imposed by μ, it is expected that μ will also significantly affect the composition of the phase diagram. As a result, we chose to construct the phase diagrams for different values of μ and R. The phase diagrams are constructed corresponding to those values of R, which shows a reasonable amount of change in the topology of the phase diagrams.

For a smaller value of μ, i.e., $\mu = 0.1$, Fig. 2(a) illustrates the phase diagram for a smaller value of R consisting of two distinct phases, the LD and LD-HD phases. The LD phase dominates the phase plane, and an LD-HD phase only appears for the smaller values of β. This can be explained as follows: the system's scarcity of particles leads to a reduced effective entry rate. As a result, the phase plane mostly exhibits an LD phase. But for smaller values of β, the exit of the particle is hindered, causing a boundary layer that enters the lattice in the form of a stationary shock. It is also evident that as the value of R increases in the range (0,5), it causes the boundary layer to exit the bulk of the lattice. This, in turn, leads to a shrinkage in the LD-HD phase and an expansion in the LD phase. For $R = 5$, the LD-HD phase completely vanishes and the LD phase covers the whole space in the phase diagram. For $R > 5$, the resetting phenomena cause the MC phase to begin appearing in the phase diagram. These findings are in contrast with the conventional TASEP (without resetting) in the presence of finite resources. The further increase in the value of R observes no significant topological changes in the phase plane except for the shift in the phase boundary due to the expansion of the MC phase and the shrinkage of the LD phase. For larger values of R, the phase plane is mostly dominated by the MC phase.

For a relatively larger value of μ, i.e., $\mu = 0.3$, the phase diagram for $R \in [0, 1]$ behaves similarly corresponding to the smaller value of μ as shown in Fig. 3(a). As R increases from 1, two more phases, namely MC and MC-HD, also join the phase diagram for larger values of α; see Fig. 3(b). Contrary to the case $R \in [0, 1]$, the LD phase shrinks for $R > 1$, whereas the MC phase and MC-HD phase expand; see Fig. 3(c). As R increases, the MC phase continues to expand, whereas the rest of the three phases (the LD phase, LD-HD phase, and MC-HD phase) shrink, and finally, for $R = 5$, the LD-HD phase completely vanishes from the phase diagram leaving behind four stationary phases: LD, MC, and MC-HD phases. The further increase in the value of R causes further expansion of the MC phase, whereas both the LD phase and the MC-HD phase continue to shrink. Moreover, in contrast to the phase diagram of TASEP-LR corresponding to infinite resources [63], we also observe a transition in the stationary phase from the LD-HD phase to the LD phase and further to the MC phase in the phase diagram corresponding to $\mu = 0.3$ and $R = 1.5$; see Fig. 6(a).

When the total number of particles in the system is the same as the number of lattice sites is considered, i.e., $\mu = 1$, the phase diagram for a smaller value of R becomes much richer as compared to the case $\mu < 1$. Here, the MC phase appears for much smaller values of R in contrast to the case $\mu < 1$. Moreover, a new stationary phase, namely, the HD phase also appears in the phase diagram for a very smaller

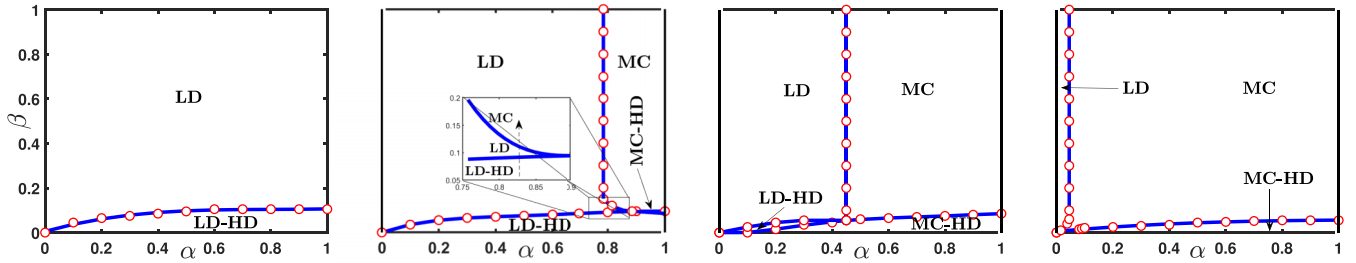

(a) $R = 1$ (b) $R = 1.5$ (c) $R = 2$ (d) $R = 5$

FIG. 3. Stationary state phase diagrams for $\mu = 0.3$ and different values of R. The markers are results from Monte Carlo simulations (MCS) and the solid lines are results from a continuum mean-field (CMF) approximation. The transition from MC to the MC-HD phase is discontinuous, whereas in panel (c), the transition from LD-HD to the MC-HD phase displays a continuous transition.

value of R which was not observed earlier ($\mu < 1$) for any value of R; see Fig. 4(a). Increasing the value of R to 0.25 leads to the formation of an additional phase, MC-HD phase and as a result, the phase diagram exhibits all possible five stationary phases as shown in Fig. 4(b). The subsequent rise in the value of R up to 1 causes contraction in the LD phase, LD-HD phase, and HD phase, whereas the MC phase and the MC-HD phase expand; see Fig. 4(c). For larger values of R, the LD-HD phase vanishes completely and the MC phase continues to expand whereas now MC-HD phase also contracts along with the LD and HD phases; see Fig. 4(d). Finally, we discuss the impact of the resetting rate for the larger value of μ. For the sake of simplicity, we assumed $\mu = 10$ and observed that now even for a very small R, the phase diagram consists of all possible five stationary phases; see Fig. 5(a). The effect of increasing R remains the same as discussed for previous cases; see Figs. 5(b), 5(c), and 5(d).

As a result, after carefully examining the phase diagrams for different values of μ and R, we discuss the stationary state features in both the small and large resetting scenarios. In the small resetting regime, the resetting rate r vanishes faster than $1/L$, which makes it simple to verify that the stationary state phase diagram trivially reduces to that of a conventional TASEP with finite resources. In the latter case (large resetting regime), the resetting dominates over the injection, extraction as well as hopping process, and the phase diagram is mostly occupied by the MC phase. To validate this, Fig. 6(b) illustrates a density profile in the large resetting regime corresponding to a specific parameter choice. It exhibits both finite-difference and Monte Carlo results of a stationary density profile for increasingly large and finite-size L which is characterized by $\rho_1 \to 1$ and $\rho_L \to 0$. The numerical inspection suggests that the bulk density profile for $L \to \infty$ is similar to the MC phase. To support this statement, the analytically obtained stationary density profile for the MC phase in Eq. (12) is written as a function of a scaled position variable $\xi = \lambda i/L$. Hence, Fig. 6(b) clearly shows that the analytically obtained expression for the MC phase profile matches with the Monte Carlo results.

B. Influence of R and μ on stationary state density and current

In this section, we will scrutinize the impact of the resetting rate and filling factor on the stationary state density profiles and the current in the system. Initially, for a fixed choice of μ, we examine the significance of the resetting rate on the density, followed by an analysis of the exit, entry, and bulk current in the system, as shown in Fig. 7(a). The top and the bottom panels in Fig. 7(a) illustrates the density profile and the current across the lattice, respectively, for a fixed μ and varying R. With an increase in R, the left end density of the lattice increases while the right end density decreases. This can also be explained as follows: when the reset rate is high, the particles at the bulk or the exit site detach easily and attach to the first site leading to an increase in the density at the entry. The bulk density profile exhibits a nonmonotonic behavior with respect to R. The density in the left part of the lattice increases, while the density in the right part decreases. From the bottom panel, it is evident that an increase in the resetting

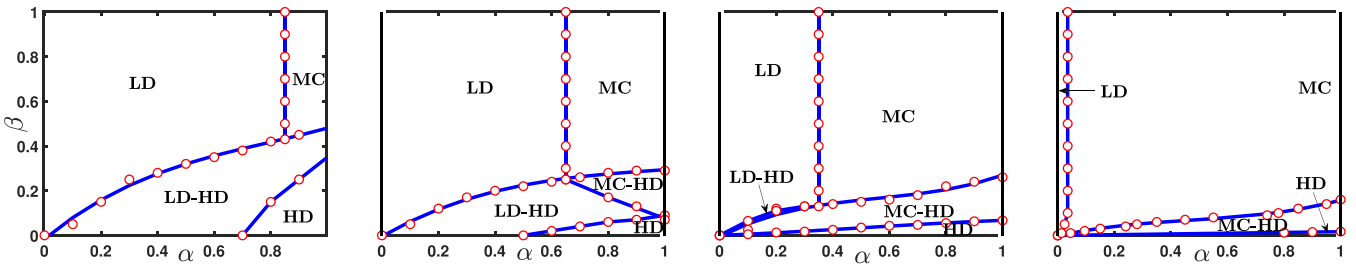

(a) $R = 0.03$ (b) $R = 0.25$ (c) $R = 1$ (d) $R = 5$

FIG. 4. Stationary state phase diagrams for $\mu = 1$ and different values of R. The markers are results from Monte Carlo simulations (MCS) and the solid lines are results from a continuum mean-field (CMF) approximation. The transition from LD-HD as well as the MC-HD phase to the HD phase is discontinuous.

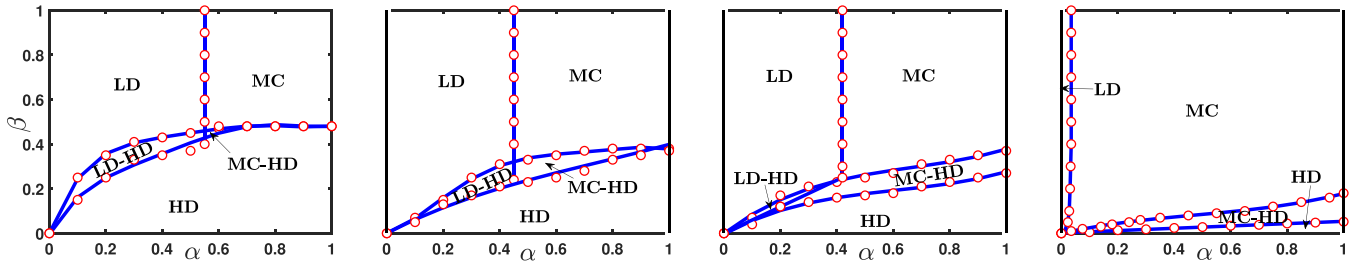

(a) $R = 0.03$ (b) $R = 0.25$ (c) $R = 0.5$ (d) $R = 5$

FIG. 5. Stationary state phase diagrams for $\mu = 10$ and different value of R. The markers are results from Monte Carlo simulations (MCS) and the solid lines are results from continuum mean-field (CMF) approximation.

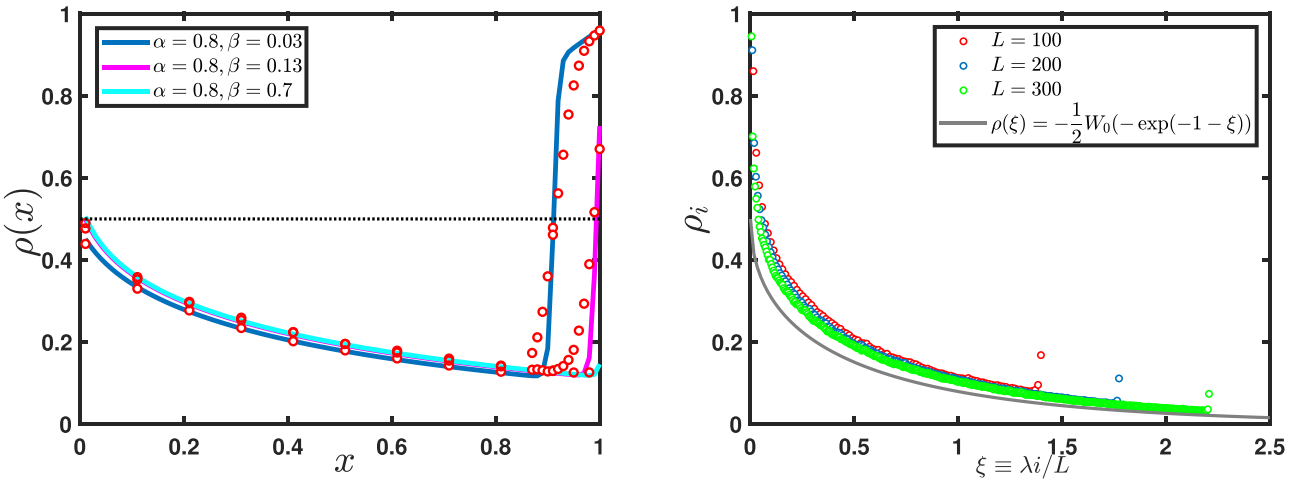

(a) $\alpha = 0.5, \beta = 0.2$ (b) $\alpha = 0.7, \beta = 0.4$

FIG. 6. (a) Transition of the stationary state density profile from the LD-HD phase to the LD phase and thereafter to the MC phase for $\mu = 0.3, R = 1.5$. The black dotted line is marked to show $\rho = 0.5$. (b) Stationary density profile as a function of the scaled position variable $\xi \equiv \lambda i/L$, in the large resetting regime: $r = R/L = 0.1$ and $\mu = 1$. The solid lines denote the mean-field continuum profile and the markers denote Monte Carlo results.

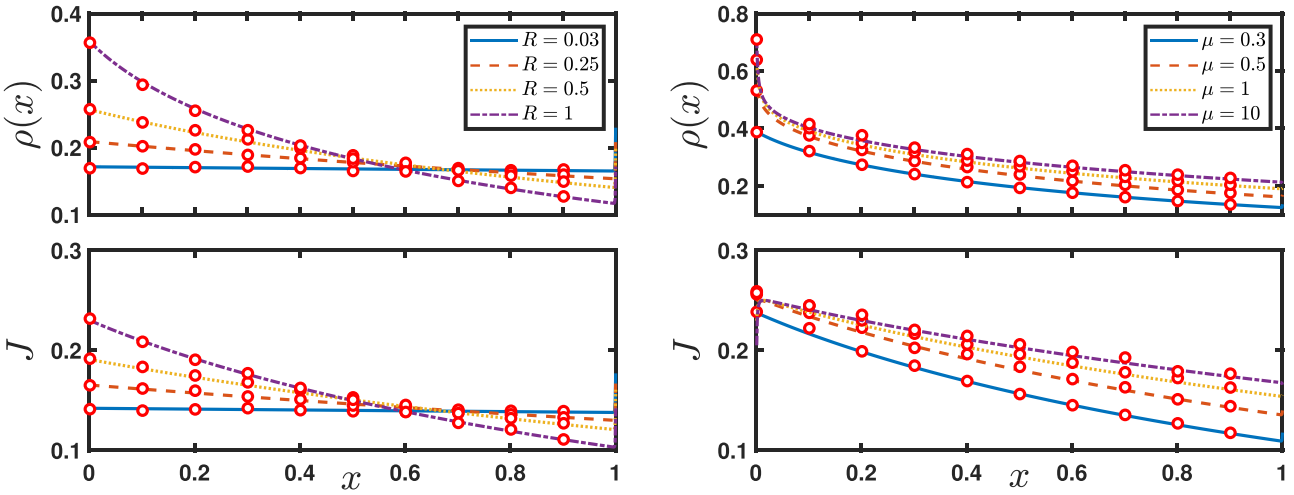

(a) $\alpha = 0.2, \beta = 0.6, \mu = 1$ (b) $\alpha = 0.6, \beta = 0.8, R = 1$

FIG. 7. Stationary state density and current displaying (a) the effect of R and (b) the effect of μ. The markers represent outcomes obtained through Monte Carlo simulations (MCS), while the solid lines depict results derived from the continuum mean-field (CMF) approximation.

rate results in a decrease in the exit current, whereas the entry current increases. Conversely, the bulk current increases in the left segment of the lattice and decreases in the right segment with an increase in the resetting rate. The resetting rate induces similar effect on both the stationary state density and current due to a relationship between them.

Subsequently, we explore the effect of the filling factor for a fixed choice of the resetting rate on the density as well as current, as illustrated in Fig. 7(b). The effect of μ is shown on the density profile and the lattice current, respectively, in the top and bottom panels of Fig. 7(b). Unlike the previous case, it is evident from the top panel that as μ increases, the density increases uniformly throughout the lattice. This can be argued as: with the increase in the filling factor, there is an increase in the average number of particles available for each site resulting in a uniform increase in the density of the lattice. It is also evident from the top panel of Fig. 7(b) that the increase in the average densities is reasonable when μ increases from 0 to 1. For further increase in the μ, the sufficient particles enter the lattice resulting in the saturation of the density profile. Finally, it converges to the one corresponding to the resetting model for infinite resources as $\mu \to \infty$ [63]. The bottom panel reveals that all entry, bulk, and exit currents increase relative to the filling factor which is in accordance with the correlation between the current in the system and its densities.

C. Comparison of the proposed model with TASEP-LK detachment only

Due to the local resetting of particles from all the bulk sites to the entry site, the proposed model can be thought of as a special TASEP-LK model with detachment-only [57]. Now, we will swiftly discuss this connection. For low values of the detachment rate, the phase diagram in the Ref. [57] also contains the same set of five stationary phases as we observed in the proposed model: LD, HD, MC, LD-HD, and MC-HD. As the detachment rate increases, there is a loss of particles from the bulk of the lattice leading to the expansion of the LD and MC phase and the HD phase shrinks whereas the LD-HD phase and the MC-HD phase expand initially. As the detachment rate is increased to a certain threshold value, the phase diagram in Ref. [57] stops exhibiting the HD phase whereas the LD-HD phase and MC-HD phase begin to contract beyond this value while the LD and the MC continue to expand. Last, for large values of the detachment rate, the phase diagram becomes equally occupied by both LD and MC phases about the transition line at $\alpha = 1/2$.

In contrast, Fig. 5 of the proposed model for larger values of μ illustrates that the region containing LD-HD phase shrinks from the beginning itself along with the HD phase whereas only the MC-HD phase expands together with the growth of the MC phase as the resetting rate increases. It appears that the HD phase occurs for even high values of the resetting rate, in contrast to the scenario in Ref. [57], albeit existing in a relatively tiny region. Additionally, for large values of the resetting rate, the particles free themselves from the bulk of the lattice to re-enter the lattice and making the effective entry rate larger. Therefore, only the MC phase dominates the phase diagram in the resetting model, however, the rest of the phases shrink.

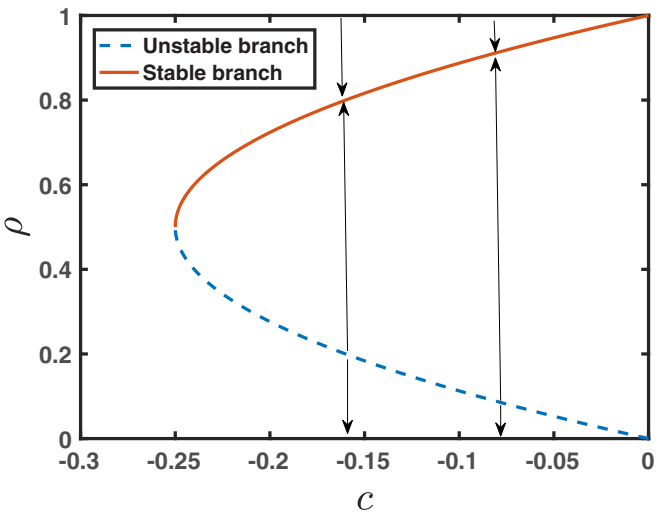

FIG. 8. Fixed-point diagram.

D. Shock dynamics and finite-size effect

Now, we discuss the features of the localized shock that appear either in the LD-HD phase or MC-HD phase where the position of the shock does not vary stochastically with respect to time. The stationary density profiles for the LD-HD (MC-HD) shock exhibit a low-density (maximal-current) profile on the left and a high-density profile on the right, separated by a domain wall or shock. Both these shocks are categorized as upward shocks since the density profile on the left end of the domain wall connects to a high density on the right end. Note that our system cannot possess any downward shock, which can be justified by utilizing fixed point theory [64]. Assuming the nonconserving terms to be zero, the integration of Eq. (4) gives

$$\frac{\epsilon}{2}\frac{\partial \rho}{\partial x} - \rho(1-\rho) = c, \tag{24}$$

where c is the integration constant. Figure 8 illustrates the two-dimensional fixed-point diagram in the c-ρ plane that is obtained from the fixed points of Eq. (24). It shows that no point on the upper (unstable) branch of this curve can be connected to a point in the lower (unstable) branch utilizing a vertical line.

The implicit expression for the stationary state density profile, the position and the height of the domain wall has been obtained in Sec. III. Now, we study the impact of the resetting rate on the shock profiles starting with the LD-HD profile. Figure 9(a) shows that both the height and the position of the LD-HD shock profile change with respect to the resetting rate. The top panel of Fig. 9(b) shows the nonmonotonic behavior of the height of the LD-HD shock with respect to the resetting rate. The shock height initially decreases up to some critical value of the resetting rate and increases afterward. However, the position of the LD-HD shock monotonically increases with the resetting rate [see bottom panel of Fig. 9(b)]. Initially, the position of the domain wall increases linearly with R and

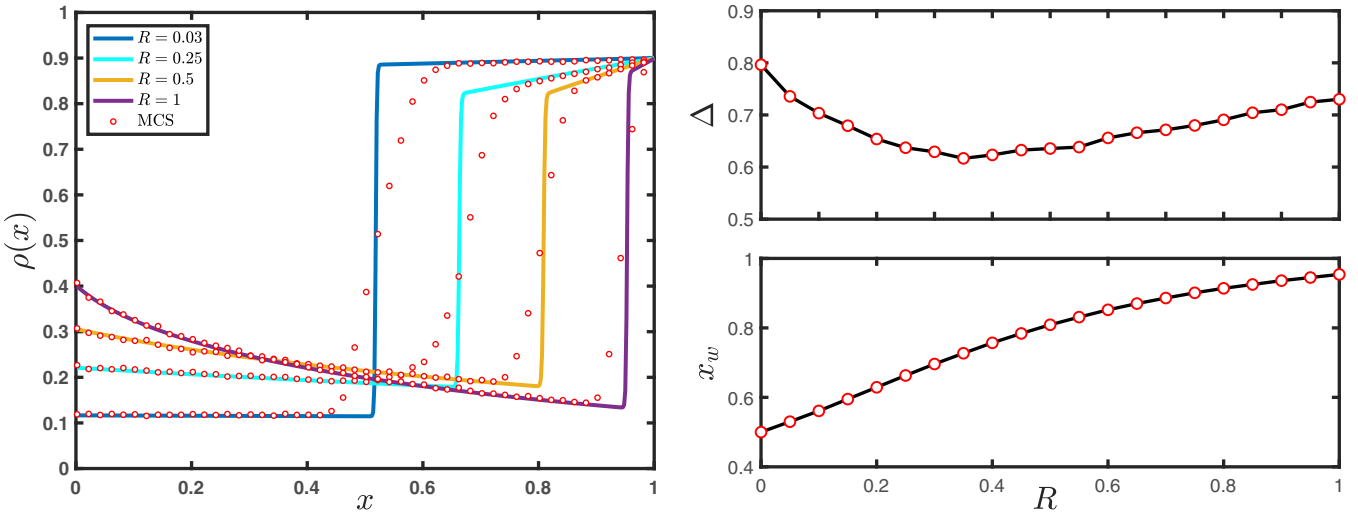

(a) (b)

FIG. 9. Effect of R on the (a) LD-HD shock profile and (b) its height and position for $\mu = 1$ and $\alpha = 0.2$, $\beta = 0.1$.

saturates to 1 as the shock exits from the right end of the lattice. This finding can be validated by the phase diagram, where the transition of the LD-HD phase to the LD phase occurs with an increase in the resetting rate. The effect on the shock in the MC-HD phase with respect to the resetting rate is illustrated in Fig. 10(a). Clearly, both the height and the position of the shock change with respect to R. In the MC-HD phase, the position as well as the height of the shock show a monotonic increasing behavior with R before saturating, see Fig. 10(b).

Last, we examine the finite-size effect on the shock profiles. We have plotted the density profiles for a point in the LD-HD region as well as the MC-HD region with $\mu = 1$ and for different values of L (see Fig. 11). As expected, the shock profile is primarily sharpened by an increase in the value of L, proving that no finite-size effect occurs in our system.

VII. CONCLUSION

Motivated by the biological process of mRNA translation where the resetting dynamics models the observed stochastic decay of mRNA-ribosome machinery, involve lanes whose dynamics depend on competition for a pool of limited particles. Hence, we made an effort to extensively investigate the characteristics of a single-channel TASEP with stochastic local resetting in a resource-constrained environment. To study the stationary state of a TASEP-LR where local resetting occurs at the entry node, we used the mean-field approximation to solve the master equations in the continuum limit and determine the explicit expression of the density profiles in terms of a Lambert-W function. The existence region of the stationary phases is obtained numerically using finite difference schemes. All these steady-state characteristics such as phase diagrams, and particle density accord very

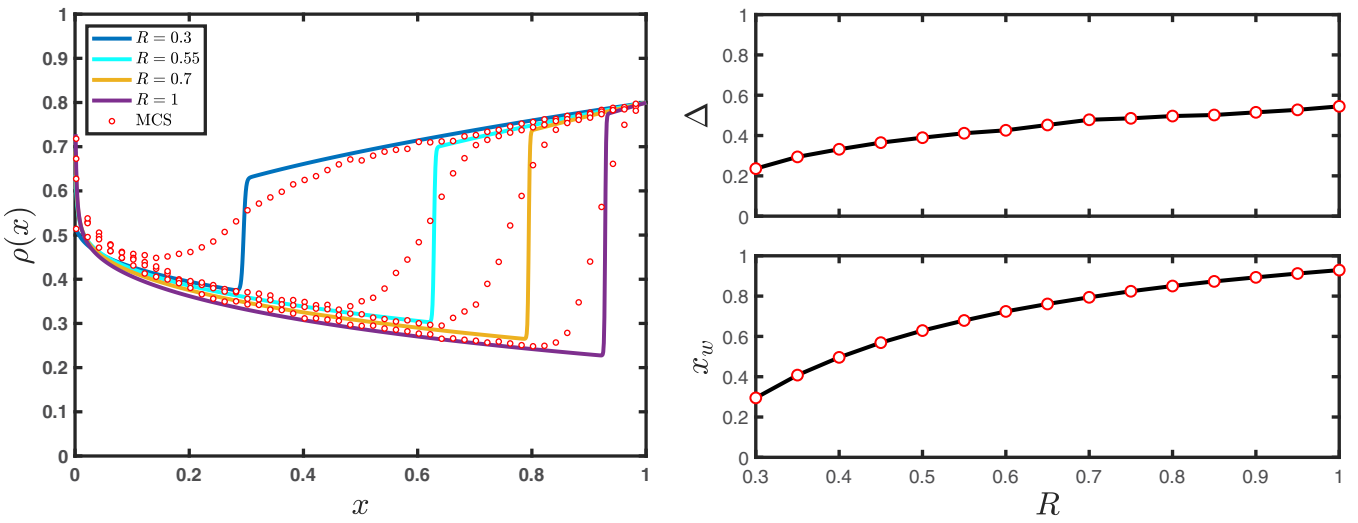

(a) (b)

FIG. 10. Effect of R on the (a) MC-HD shock profile and (b) its height and position for $\mu = 1$ and $\alpha = 0.9$, $\beta = 0.2$.

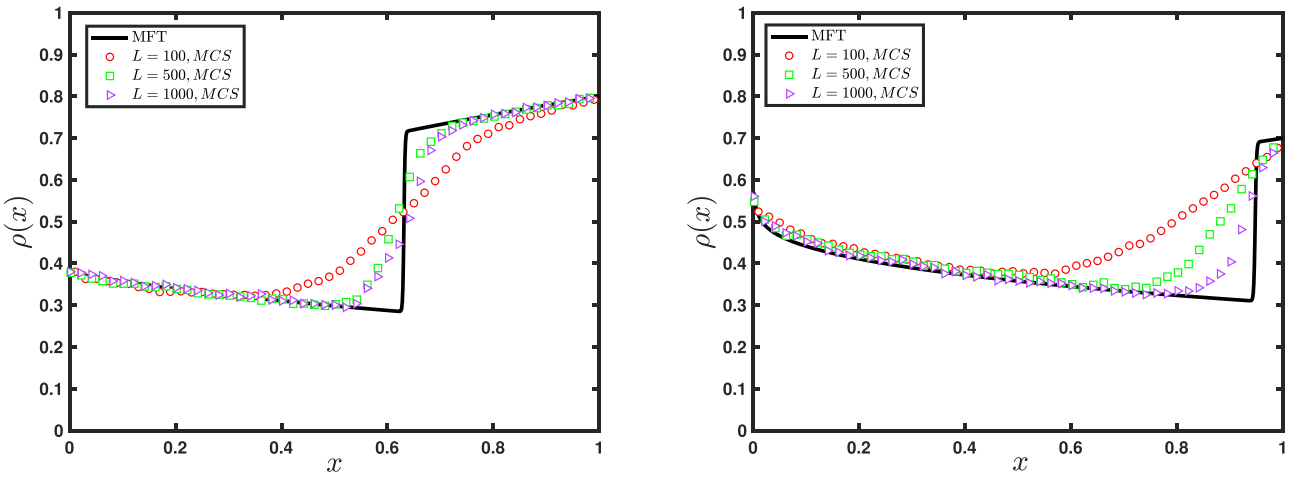

(a) $\alpha = 0.5, \beta = 0.2$ (b) $\alpha = 0.8, \beta = 0.3$

FIG. 11. Finite-size effect on (a) the LD-HD density profile as well as (b) the MC-HD density profile for $\mu = 1$ and $R = 0.25$.

well with the Monte Carlo simulations in the thermodynamic limit.

The total number of particles remains constant in the system and is characterized by the filling factor. Another important factor is the macroscopic resetting rate, whose behavior in the thermodynamic limit $L \to \infty$ establishes the significance of the resetting process. While the filling factor intends to investigate the influence of the total number of particles on the system dynamics. We scrutinized the stationary properties of the system for different choices of the filling factor while scaling the resetting rate simultaneously. The phase diagram has the possibility of the following five stationary phases: the LD phase, the MC phase, the HD phase, the LD-HD phase, and the MC-HD phase depending upon the choice of the filling factor and resetting rate. In the large resetting regime, the phase diagram becomes completely dominated by the MC phase irrespective of the choice of the filling factor. In contrast to the standard TASEP with finite resources, the proposed model for smaller values of the filling factor possesses an MC phase whereas the LD-HD phase vanishes completely in the intermediate as well as large resetting regime. However, as soon as the resetting rate vanishes, the phase diagram of the proposed model behaves likewise to the standard TASEP with finite resources. In contrast to the resetting model corresponding to infinite resources [63], we observe two new phase transitions which arguably induce a change in the topology of the phase diagram. The first phase transition has been observed for a smaller value of the filling factor and an intermediate choice of the resetting rate. It occurs in the following manner: LD-HD $\to$ LD $\to$ MC phase whereas the second phase transition is observed when the system has a number of particles equivalent to the lattice size with an intermediate resetting rate, it takes place as follows: HD $\to$ LD-HD $\to$ MC-HD $\to$ MC phase. We also established a relationship with the TASEP-LK detachment-only model, where the stationary properties of both models have been compared. Lastly, we investigated the role of the resetting rate on the shock dynamics and examined the finite-size effect on their stationary state properties.

Now, we conclude the proposed theoretical work with its potential applications in the microscopic realm of biological systems where the conventional TASEP describes the ribosome dynamics. While the model is generic in nature, it holds versatile potential for applications in situations involving the attachment or detachment of particles. For instance, it has the capability to simulate the dynamic facets of phenomena such as the drop-off phenomenon. This refers to the premature halt of the translation process caused by stalled ribosomes, encompassing their subsequent rescue and recycling processes [30,57,58]. The work can be extended to incorporate more realistic features related to diverse physical and biological systems.

[1] K. Nagel, Particle hopping models and traffic flow theory, Phys. Rev. E **53**, 4655 (1996).

[2] M. Schreckenberg, A. Schadschneider, K. Nagel, and N. Ito, Discrete stochastic models for traffic flow, Phys. Rev. E **51**, 2939 (1995).

[3] A. Schadschneider, D. Chowdhury, and K. Nishinari, *Stochastic Transport in Complex Systems: From Molecules to Vehicles* (Elsevier, Amsterdam, 2010).

[4] V. Belitsky, J. Krug, E. J. Neves, and G. M. Schütz, A cellular automaton model for two-lane traffic, J. Stat. Phys. **103**, 945 (2001).

[5] E. T. Jaynes, Gibbs vs Boltzmann entropies, Am. J. Phys. **33**, 391 (1965).

[6] D. Chowdhury, L. Santen, and A. Schadschneider, Statistical physics of vehicular traffic and some related systems, Phys. Rep. **329**, 199 (2000).

[7] J. Krug, Boundary-induced phase transitions in driven diffusive systems, Phys. Rev. Lett. **67**, 1882 (1991).

[8] S. Katz, J. L. Lebowitz, and H. Spohn, Phase transitions in stationary nonequilibrium states of model lattice systems, Phys. Rev. B **28**, 1655 (1983).

[9] F. Spitzer, Interaction of Markov Processes, in *Random Walks, Brownian Motion, and Interacting Particle Systems: A Festschrift in Honor of Frank Spitzer* (Birkhäuser, Boston, MA, 1991), pp. 66–110.
[10] A. B. Kolomeisky, G. M. Schütz, E. B. Kolomeisky, and J. P. Straley, Phase diagram of one-dimensional driven lattice gases with open boundaries, J. Phys. A: Math. Gen. **31**, 6911 (1998).
[11] G. M. Schütz, Exactly solvable models for many-body systems far from equilibrium, in *Phase Transitions and Critical Phenomena* (Academic Press, San Diego, CA, 2001), Vol. 19, pp. 1–251.
[12] M. E. Foulaadvand and P. Maass, Phase transitions and optimal transport in stochastic roundabout traffic, Phys. Rev. E **94**, 012304 (2016).
[13] T. Chou and G. Lakatos, Clustered bottlenecks in mRNA translation and protein synthesis, Phys. Rev. Lett. **93**, 198101 (2004).
[14] A. Schadschneider, Traffic flow: A statistical physics point of view, Physica A **313**, 153 (2002).
[15] S. Klumpp and R. Lipowsky, Traffic of molecular motors through tube-like compartments, J. Stat. Phys. **113**, 233 (2003).
[16] R. Lipowsky, S. Klumpp, and T. M. Nieuwenhuizen, Random walks of cytoskeletal motors in open and closed compartments, Phys. Rev. Lett. **87**, 108101 (2001).
[17] J. de Gier and F. H. Essler, Bethe ansatz solution of the asymmetric exclusion process with open boundaries, Phys. Rev. Lett. **95**, 240601 (2005).
[18] D. Simon, Construction of a coordinate Bethe ansatz for the asymmetric simple exclusion process with open boundaries, J. Stat. Mech. (2009) P07017.
[19] Q. Y. Hao, R. Jiang, M. B. Hu, C. Y. Wu, and N. Guo, Analytical investigation on totally asymmetric simple exclusion process with Langmuir kinetics and a parallel update with two sub-steps, Chaos Solitons Fractals **160**, 112233 (2022).
[20] D. Chowdhury, A. Schadschneider, and K. Nishinari, Physics of transport and traffic phenomena in biology: from molecular motors and cells to organisms, Phys. Life Rev. **2**, 318 (2005).
[21] B. Derrida, An exactly soluble nonequilibrium system: the asymmetric simple exclusion process, Phys. Rep. **301**, 65 (1998).
[22] G. Schütz and E. Domany, Phase transitions in an exactly soluble one-dimensional exclusion process, J. Stat. Phys. **72**, 277 (1993).
[23] D. Helbing, Traffic and related self-driven many-particle systems, Rev. Mod. Phys. **73**, 1067 (2001).
[24] C. T. MacDonald and J. H. Gibbs, Concerning the kinetics of polypeptide synthesis on polyribosomes, Biopolymers **7**, 707 (1969).
[25] K. Nishinari, Y. Okada, A. Schadschneider, and D. Chowdhury, Intracellular transport of single-headed molecular motors KIF1A, Phys. Rev. Lett. **95**, 118101 (2005).
[26] H. S. Kuan and M. D. Betterton, Motor protein accumulation on antiparallel microtubule overlaps, Biophys. J. **110**, 2034 (2016).
[27] J. Howard and R. L. Clark, Mechanics of motor proteins and the cytoskeleton, Appl. Mech. Rev. **55**, B39 (2002).
[28] A. Parmeggiani, T. Franosch, and E. Frey, Phase coexistence in driven one-dimensional transport, Phys. Rev. Lett. **90**, 086601 (2003).
[29] M. R. Evans, R. Juhász, and L. Santen, Shock formation in an exclusion process with creation and annihilation, Phys. Rev. E **68**, 026117 (2003).
[30] A. Parmeggiani, T. Franosch, and E. Frey, Totally asymmetric simple exclusion process with Langmuir kinetics, Phys. Rev. E **70**, 046101 (2004).
[31] M. R. Evans and S. N. Majumdar, Diffusion with stochastic resetting, Phys. Rev. Lett. **106**, 160601 (2011).
[32] A. Valleriani, Z. Ignatova, A. Nagar, and R. Lipowsky, Turnover of messenger RNA: Polysome statistics beyond the steady state, Europhys. Lett. **89**, 58003 (2010).
[33] A. Montanari and R. Zecchina, Optimizing searches via rare events, Phys. Rev. Lett. **88**, 178701 (2002).
[34] J. Q. Toledo-Marin, D. Boyer, and F. J. Sevilla, Predator-prey dynamics: Chasing by stochastic resetting, arXiv preprint arXiv:1912.02141.
[35] S. Reuveni, M. Urbakh, and J. Klafter, The role of substrate unbinding in michaelis-menten enzymatic reactions, Biophys. J. **106**, 677a (2014).
[36] É. Roldán, A. Lisica, D. Sánchez-Taltavull, and S. W. Grill, Stochastic resetting in backtrack recovery by RNA polymerases, Phys. Rev. E **93**, 062411 (2016).
[37] R. Falcao and M. R. Evans, Interacting Brownian motion with resetting, J. Stat. Mech. (2017) 023204.
[38] M. R. Evans and S. N. Majumdar, Run and tumble particle under resetting: A renewal approach, J. Phys. A: Math. Theor. **51**, 475003 (2018).
[39] S. Karthika and A. Nagar, Totally asymmetric simple exclusion process with resetting, J. Phys. A: Math. Theor. **53**, 115003 (2020).
[40] U. Basu, A. Kundu, and A. Pal, Symmetric exclusion process under stochastic resetting, Phys. Rev. E **100**, 032136 (2019).
[41] A. Miron and S. Reuveni, Diffusion with local resetting and exclusion, Phys. Rev. Res. **3**, L012023 (2021).
[42] A. Pelizzola, M. Pretti, and M. Zamparo, Simple exclusion processes with local resetting, Europhys. Lett. **133**, 60003 (2021).
[43] B. Derrida, M. R. Evans, V. Hakim, and V. Pasquier, Exact solution of a 1D asymmetric exclusion model using a matrix formulation, J. Phys. A: Math. Gen. **26**, 1493 (1993).
[44] T. L. Blasius, N. Reed, B. M. Slepchenko, and K. J. Verhey, Recycling of kinesin-1 motors by diffusion after transport, PLoS ONE **8**, e76081 (2013).
[45] L. Ciandrini, I. Neri, J. C. Walter, O. Dauloudet, and A. Parmeggiani, Motor protein traffic regulation by supply-demand balance of resources, Phys. Biol. **11**, 056006 (2014).
[46] M. Ha and M. Den Nijs, Macroscopic car condensation in a parking garage, Phys. Rev. E **66**, 036118 (2002).
[47] D. A. Adams, B. Schmittmann, and R. K. Zia, Far-from-equilibrium transport with constrained resources, J. Stat. Mech. (2008) P06009.
[48] A. Haldar, P. Roy, and A. Basu, Asymmetric exclusion processes with fixed resources: Reservoir crowding and steady states, Phys. Rev. E **104**, 034106 (2021).
[49] L. J. Cook and R. K. Zia, Feedback and fluctuations in a totally asymmetric simple exclusion process with finite resources, J. Stat. Mech. (2009) P02012.
[50] L. J. Cook, J. J. Dong, and A. LaFleur, Interplay between finite resources and a local defect in an asymmetric simple exclusion process, Phys. Rev. E **88**, 042127 (2013).
[51] C. A. Brackley, L. Ciandrini, and M. C. Romano, Multiple phase transitions in a system of exclusion processes with limited reservoirs of particles and fuel carriers, J. Stat. Mech. (2012) P03002.

[52] P. Greulich, L. Ciandrini, R. J. Allen, and M. C. Romano, Mixed population of competing totally asymmetric simple exclusion processes with a shared reservoir of particles, Phys. Rev. E **85**, 011142 (2012).

[53] S. A. Janowsky and J. L. Lebowitz, Finite-size effects and shock fluctuations in the asymmetric simple-exclusion process, Phys. Rev. A **45**, 618 (1992).

[54] A. K. Verma and A. K. Gupta, Limited resources in multi-lane stochastic transport system, J. Phys. Commun. **2**, 045020 (2018).

[55] A. K. Verma and A. K. Gupta, Stochastic transport on flexible lattice under limited resources, J. Stat. Mech. (2019) 103210.

[56] C. T. MacDonald, J. H. Gibbs, and A. C. Pipkin, Kinetics of biopolymerization on nucleic acid templates, Biopolymers **6**, 1 (1968).

[57] P. Bonnin, N. Kern, N. T. Young, I. Stansfield, and M. C. Romano, Novel mRNA-specific effects of ribosome drop-off on translation rate and polysome profile, PLoS Comput. Biol. **13**, e1005555 (2017).

[58] S. Franckenberg, T. Becker, and R. Beckmann, Structural view on recycling of archaeal and eukaryotic ribosomes after canonical termination and ribosome rescue, Curr. Opin. Struct. Biol. **22**, 786 (2012).

[59] L. Ciandrini, I. Stansfield, and M. C. Romano, Ribosome traffic on mRNAs maps to gene ontology: genome-wide quantification of translation initiation rates and polysome size regulation, PLoS Comput. Biol. **9**, e1002866 (2013).

[60] R. M. Corless, G. H. Gonnet, D. E. Hare, D. J. Jeffrey, and D. E. Knuth, On the Lambert W function, Adv. Comput. Math. **5**, 329 (1996).

[61] V. Popkov and G. M. Schütz, Steady-state selection in driven diffusive systems with open boundaries, Europhys. Lett. **48**, 257 (1999).

[62] A. Gupta, B. Pal, A. Jindal, N. Bhatia, and A. K. Gupta, Modelling of transport processes: Theory and simulations, MethodsX **10**, 101966 (2023).

[63] A. Pelizzola and M. Pretti, Totally asymmetric simple exclusion process with local resetting and open boundary conditions, J. Phys. A: Math. Theor. **55**, 454001 (2022).

[64] S. Mukherji, Fixed points and boundary layers in asymmetric simple exclusion processes, Phys. Rev. E **79**, 041140 (2009).